

pubs.acs.org/cm Article

Controlling the Formation of Charge Transfer Complexes in Chemically Doped Semiconducting Polymers

Dane A. Stanfield, Yutong Wu, Sarah H. Tolbert, and Benjamin J. Schwartz*



Cite This: Chem. Mater. 2021, 33, 2343-2356



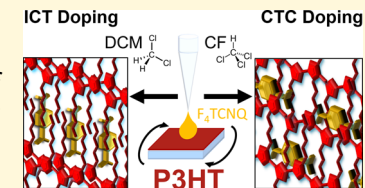
ACCESS

Metrics & More



Supporting Information

ABSTRACT: Chemical doping of semiconducting polymers predominantly takes place via integer charge transfer (ICT), where an electron is entirely removed from the host conjugated polymer and transferred to reside on the dopant guest species. In contrast, chemical doping of small conjugated molecules and oligomers often leads to the formation of charge transfer complexes (CTCs), which have significant orbital overlap and shared electron density between the host and guest species. To date, the observation of fractional charge transfer in doped conjugated polymers is relatively rare, occurring only under extreme processing conditions that



can be difficult to achieve, which is fortunate given that CTC formation generally yields fewer mobile carriers per dopant. In this work, we use the classic conjugated polymer/dopant pair of P3HT and F4TCNQ to demonstrate how simply adjusting the casting solvent for the dopant in sequential processing can fundamentally alter the nature of doping in this well-studied system, leading to tunable production of CTCs. Using solvent blends of dichloromethane and chloroform, selected for their low and high solubility toward P3HT, respectively, we show that the relative amount of polymer-dopant CTCs can be readily controlled over an order of magnitude. Increasing the amount of chloroform in the dopant solvent blend favors the creation of CTCs, while increasing the dichloromethane content results in doping by the more standard ICT; the results allow us to explain why CTC formation is common in charge-transfer salts but generally less so in doped conjugated polymers. We also explore the role of the doping method and the crystallinity of P3HT films in controlling the relative amounts of ICT and CTC formation. We find that the use of evaporation doping and higher-crystallinity material discourages CTC formation, but that even in the most favorable case of evaporation doping with high polymer crystallinity, fractional charge transfer always occurs to some extent. Finally, we show that brief thermal annealing can convert CTCs to integer charge transfer species, indicating that ICT is the thermodynamically preferred doping mechanism in conjugated polymers, and that fractional charge transfer is the result of kinetic trapping. With this understanding, we offer guidelines for limiting the occurrence of charge transfer complexes during sequential doping of conjugated polymers, thus avoiding the deleterious effects of CTCs on charge transport.

1. INTRODUCTION

Conjugated organic semiconductors offer great promise as the active materials for applications in flexible electronics, including light-emitting diodes, photovoltaics, and thermoelectric devices. 1-5 For many of these applications, it is necessary to introduce equilibrium charge carriers into the π systems of these materials. This is often achieved by chemical doping, which involves the introduction of a strong oxidizing (or reducing) agent to remove (or add) electrons from (to) an organic semiconductor. In organic light-emitting diodes and photovoltaic cells, for example, chemical doping of an interfacial conjugated polymer layer can lower barriers and enhance charge injection. Additionally, for organic thermoelectric materials, doping dramatically affects both the Seebeck coefficient and the electrical conductivity, two of the factors that comprise the thermoelectric figure of merit. 3,6,7 Most organic semiconductors are p-type materials, so they are best doped by using strong oxidizing agents to remove electrons from the π -conjugated backbone.

The idea of chemical doping of organic semiconductors has its roots in the study of charge-transfer salts, which dates back to the 1970s. 8-10 The classic example of a charge-transfer salt

is a mixture of tetrathiafulvalene (TTF) and 7,7,8,8-tetracyanoquinodimethane (TCNQ). ¹¹ In such charge-transfer salts, acceptor molecules like TCNQ act as oxidizing agents, removing part of an electron from conjugated donors like TTF. The co-crystals are characterized by charge-transfer complexes (CTCs), which result in delocalized electronic states with a band structure that has the valence band predominantly derived from the donor HOMO and the conduction band from the acceptor LUMO. ¹² Such charge-transfer salts can exhibit a metallic behavior if they form in the right co-crystal structure and have sufficient driving force for charge separation (i.e., the energetic offset between the oxidation potential of the donor and the reduction potential of the acceptor is sufficiently

Received: November 19, 2020 Revised: January 14, 2021 Published: March 5, 2021





large), both of which determine the fraction of an electron that is locally transferred from the donor to the acceptor. ^{10,13}

Unlike the donors in small-molecule charge-transfer salts, when solution-processable conjugated polymers are mixed with small-molecule oxidizing agents, the result is nearly always integer charge transfer (ICT); 14-24 the types of CTCs that are readily observed with small conjugated molecules in chargetransfer salts have been less commonly seen. 25-30 In fact, one needs to go to great lengths to produce CTCs from chemically doped conjugated polymers. For example, CTCs can be observed when the polymer and dopant are spun from a hot solution onto a pre-heated substrate²⁶ or when branched side chains are employed to force the dopant counterion into specific locations in the polymer crystal lattice.²⁷ CTCs are usually not desirable for most doped conjugated polymer applications since they produce a smaller fraction of dopinginduced carriers than ICTs; thus, their relative rarity is generally advantageous.³¹ However, it is still not clear why ICT is favored when chemically doping conjugated polymers. This leads to the central question explored in this work: why do mixtures of acceptors with small-molecule donors, including the oligomers of many common conjugated polymers, usually produce CTCs,³² while mixtures of conjugated polymers with the same acceptors usually lead to ICT?

To address this question, in this paper we re-examine the well-studied conjugated polymer, poly(3-hexylthiophene-2,5diyl) (P3HT) doped with the strong electron acceptor 2,3,5,6tetrafluoro-7,7,8,8-tetracyanoquinodimethane (F₄TCNQ) to gain new insights into the process of how conjugated polymers produce CTCs or undergo ICT upon chemical doping. We track the degree of charge transfer using a combination of UV-Visible spectroscopy, to monitor the electronic transitions produced following doping, and FTIR spectroscopy, to determine the amount of charge transferred from the polymer to the F₄TNCQ acceptor; we also monitor the structure of the doped films using 2D grazing-incidence wide-angle X-ray scattering (GIWAXS). We find that we can control the relative amounts of CTCs and ICT that take place upon F4TCNQ doping of P3HT by using a tunable blend of solvents (dichloromethane, DCM, and chloroform, CF) to infiltrate the dopant into the polymer layer via sequential processing. Using pure DCM to deposit F₄TCNQ onto pre-cast P3HT films, we see relatively little CTC formation, whereas the use of pure CF increases CTC formation by over an order of magnitude. Sequentially depositing the dopant from blends of DCM and CF allows the amount of CTC formed to be tuned anywhere in between.

With this control in hand, we now have a toolkit for studying CTC formation without resorting to extreme processing conditions or synthetically modified conjugated polymers. This allows us to explore how different aspects of the materials and processing conditions affect the tendency to undergo CTC formation. In particular, we compare the use of evaporation doping (i.e., subliming the $\rm F_4TCNQ$ dopant onto pre-cast conjugated polymer film) 33 to the typical solution-based sequential doping method to investigate the role of dopant transport on CTC formation. We then study the role of the pre-formed polymer film crystallinity to elucidate the preference of crystalline and amorphous polymer domains to participate in CTC formation.

P3HT films are always composed of some combination of crystalline and amorphous regions, and we find that the more crystalline a P3HT film is prior to sequential doping, the

smaller the fraction of CTC states generated. However, we also find that CTC doping cannot be entirely eliminated, even for the most crystalline P3HT films, showing that there is still room to improve sequential doping methods. We also show that doping via vapor transport produces a smaller fraction of CTC states relative to solution sequential doping, providing significant clues to the role of kinetics in forming CTC states.

The structure of most conjugated polymers consists of semicrystalline regions characterized by a π -stacking spacing between the polymer backbones and a lamellar spacing along the polymer side chains. We and other research groups have argued in previous works that dopant molecules prefer to reside in the polymer lamellae as the barrier to dopant insertion into the easily disordered side chains is lower than breaking up the polymer π -stacks to insert the dop-ant. Placing dopants in the lamellae, where they reside far from the polymer backbone, leads to ICT, as there is insufficient wave function overlap between the donor and acceptor for CTC formation to take place. Instead, CTC states only occur when the F_4TCNQ dopant is able to π -stack with the conjugated polymer. 26-30 These results lead us to an improved picture of the kinetic competition between the two doping mechanisms, where the choice of processing conditions can alter the kinetic barrier for placing dopants in the polymer π -stacks. All of the results explain how solvent blends and polymer crystallinity can control the preference for ICT vs CTC formation in doped conjugated polymers, and why CTC is the preferred doping mechanism in small-molecule charge-

Finally, we show that ICT is not only kinetically preferred but is also thermodynamically favored for the $F_4TCNQ/P3HT$ combination of dopant and conjugated polymer. By exposing doped films to brief thermal annealing treatments, we find that the fraction of CTCs produced upon doping can be converted to ICT, further indicating that CTCs are kinetically trapped in doped conjugated polymer films. Overall, our work shows the steps that can be taken to minimize CTC formation for electronic applications (or to enhance CTC formation for study), including increasing the polymer crystallinity and using dopants that physically cannot π -stack or have wave function mixing with the conjugated polymer backbone. ^{21,23}

2. EXPERIMENTAL SECTION

- **2.1. Materials.** Electronic-grade P3HT (4002-EE; 91–94%, $M_{\rm w}=46-57$ kg/mol, PDI = 2.3) was purchased from Rieke Metals, and sublimation-grade F₄TCNQ (purity, >98%) was purchased from TCI America. The synthesis and preparation of the P3HT denoted "100% RR" has been described by us in prior work.²¹ All materials and solvents were used as received without any further purification.
- **2.2. Fabrication and Doping of Polymer Films.** Glass and silicon substrates were first degreased by sequentially sonicating for 10 min in a detergent solution, deionized water, acetone, and finally isopropyl alcohol. Substrates were then dried and stored in a nitrogen glove box where all subsequent solution processing steps takes place. For experiments using doping solvent blends, thin films of P3HT were prepared by spin-coating a polymer solution (20 mg mL⁻¹) out of odichlorobenzene (ODCB) at 1000 rpm for 20 s. Directly after spin-coating, the still wet films were moved to an open Petri dish until they finished drying. All dopant solutions of F₄TCNQ (1 mg mL⁻¹) for the set of solvent blends containing chloroform (CF) and dichloromethane (DCM) were generated by adding the desired volume of each solvent to a vial with F₄TCNQ powder. Sequential doping was carried out by pipetting dopant solution solvent blends (100 µL) onto pristine P3HT films and spin-coating at 4000 rpm for 10 s to remove

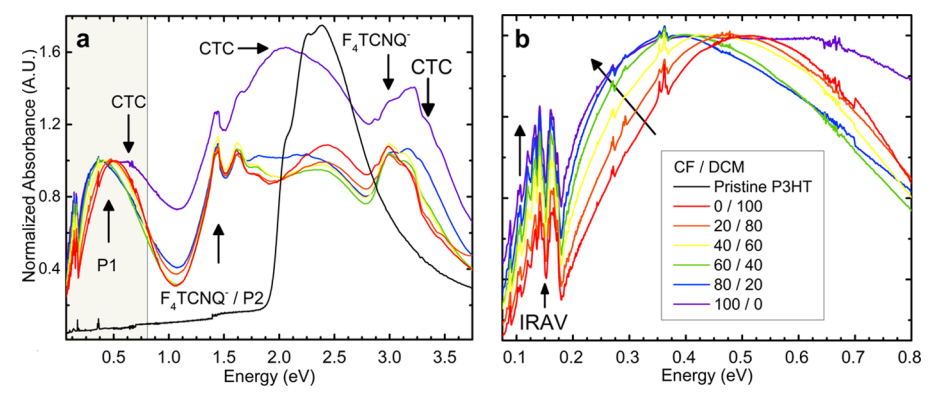


Figure 1. (a) UV-vis-NIR absorption spectrum of 1 mg mL⁻¹ F₄TCNQ sequentially doped P3HT films with the dopant deposited from solvent blends with different CF/DCM ratios, normalized to the peak absorption for the main P1 band near 0.4 eV. The electronic transitions from the CTC phase are labeled, along with the standard absorption features that appear with ICT. For comparison, the black curve shows the absorption of a P3HT film prior to doping, scaled to the correct relative absorption intensity of the film doped using 100% DCM (red curve). (b) The NIR P1 polaron absorption on an expanded energy scale of P3HT films sequentially doped with F₄TCNQ from solvent blends with the indicated CF/DCM ratio by volume; this data corresponds to the section shaded in gray in panel (a). The black arrows highlight the increased intensity of the IRAV band and the monotonic redshift of the main P1 peak absorption with increasing CF content of the dopant casting solvent, indicative of increased polaron delocalization. The absorbance for pristine P3HT is essentially zero in this part of the spectrum and has thus been omitted for clarity.

the excess material. Additional experimental details can be found in the Supporting Information.

For the experiments comparing the vapor and solution sequential doping methods, 110 and 400 nm-thick pristine P3HT films were prepared by spin-coating from 20 and 50 mg mL⁻¹ ODCB solutions respectively at 1000 rpm for 60 s followed by 3000 rpm for 5 s. Sequential solution doping with F4TCNQ was carried out by pipetting 100 μ L of dopant solution out of DCM (1 mg mL⁻¹) onto pristine P3HT films and spin-coating at 4000 rpm for 10 s to remove the excess material. Sequential vapor doping with F₄TCNQ was carried out using an Angstrom Engineering Nexdep Physical Vapor Deposition System. The F₄TCNQ powder was placed in an alumina crucible and evaporated at 0.5 Å s⁻¹ with a base pressure of $< 1 \times 10^{-6}$ Torr. Pristine P3HT films were placed on a rotating stage that was actively cooled to 15 °C during deposition. Doping levels for the vapor process were optimized to produce the highest conductivity and to show comparable doping levels to the solution-processed samples. A more detailed discussion can be found in our previous work³³ and its supporting information.

For our work comparing doped P3HT films with tunable crystallinity, we used solvent evaporation kinetics to control the rate of P3HT film formation, where higher-boiling point solvents yield higher-crystallinity polymer films. To obtain P3HT films with relatively low crystallinity, P3HT solutions (10 mg $\rm mL^{-1}$) were spin-coated from chloroform (CF) (b.p. = 61.2 °C) at 1000 rpm for 60 s. For films of intermediate crystallinity, P3HT solutions (20 mg mL^{-1}) were spin-coated from o-dichlorobenzene (ODCB) (b.p. = 180 °C) at 1160 rpm for 20 s. These still wet films were then placed in a covered Petri dish to further extend the drying period. Finally, for films with the highest degree of crystallinity, an in-house batch of P3HT with a regioregularity of essentially unity was employed. The same spin-coating procedure was used for this material as for the commercial material cast from ODCB with the exception that solutions were spin-coated out hot at 60 °C to prevent aggregation. Additional details on film preparation, synthesis, and characterization can be found in our earlier work²¹ and its supporting information.

2.3. GIWAXS Measurements of Doped Polymer Films. 2D GIWAXS data were collected at the Stanford Synchrotron Radiation Lightsource using beamline 11-3. The beam wavelength was $0.9742 \, \text{Å}$, and the incidence angle was 0.12° . The sample chamber was flowed with helium to reduce noise, and the sample holder was 250 mm away from the detector. All the samples were irradiated for 90 s. To reduce the 2D diffractograms, we used the WAXStools in Igor Pro. The diffractograms were radially integrated to reduce to 1D diffraction curves $(0-10^{\circ}$ for out-of-plane, $80-90^{\circ}$ for in-plane, and $0-90^{\circ}$ for full). All the samples at a given doping condition were made and

measured in triplicate to ensure the reproducibility and absolute scattering intensity. All diffractograms were thickness-normalized (after background subtraction) to the polymer film thickness prior to doping with F_4TCNQ since only the polymer contributes to the diffraction intensity. Additional details can be found in the Supporting Information.

3. RESULTS AND DISCUSSION

One of the most common ways to produce chemically doped polymer films is by solution sequential processing, where the dopant is infiltrated into a pre-cast conjugated polymer film using a semi-orthogonal solvent that swells but does not dissolve the underlying morphology. 17,21 Sequential doping is generally preferred because simply mixing the polymer and dopant together results in solution-phase charge transfer, creating a salt with unfavorable solubility in the non-polar organic solvents typically used to dissolve conjugated polymers. The resulting blend solutions are usually highly aggregated, leading to poor quality when cast into films. Sequential processing avoids this difficulty because the doped films largely have the same morphology as the original pre-cast films, providing the added advantage that the pre-cast polymer films can be created with different degrees of crystallinity 17,21 or rubbed to produce alignment of the polymer chains. 7,22,34 Sequential doping can also involve thermally evaporating the dopant onto a pre-cast polymer film, 20,35-39' which allows for effective infiltration of the dopant, even into polymer films that are hundreds of nanometers thick.³

3.1. Optical Transitions of P3HT: F_4 TNCQ Charge-Transfer Complexes. When using solution sequential processing to dope a conjugated polymer, the solvent selected to introduce the dopant is usually chosen to have poor solubility for the underlying polymer; however, in principle, any solvent with a reasonably high solubility for the dopant can be used. For the P3HT/ F_4 TCNQ system, we have shown that DCM is a particularly good solvent for solution sequential processing due to its reasonably high solubility toward F_4 TCNQ and relatively low solubility (0.818 mg mL $^{-1}$) toward P3HT. 17,21,33,40,41

Based on this idea, it would seem that a solvent like CF, which has one of the highest known solubilities toward P3HT

(38 mg mL⁻¹),⁴⁰ would be a poor choice for doping via solution sequential processing. This is because, at first glance, CF would be expected to dissolve the underlying polymer and thus remove the entire P3HT film from the substrate during the doping process. What we will show below, however, is that, when sequentially doping P3HT, the high dissolving power of CF does put some of the underlying P3HT film into solution while the F₄TCNQ is being introduced, effectively removing any kinetic barriers to placing the dopant in the polymer π -stacks. At the same time, the rapid decrease in polymer solubility that occurs upon doping still allows most of the polymer material to remain intact on the substrate through a dynamic dissolution and reprecipitation process.

Our first sign that using CF to sequentially dope P3HT with F_4TCNQ produces a different electronic species comes from UV–Vis–NIR spectroscopy. Figure 1 shows the results when DCM, CF, and various blends of the two solvents (which are miscible) are used to expose pre-cast films of P3HT to 1 mg mL⁻¹ solutions of F_4TCNQ . The full spectra are plotted in Figure 1a, with the IR region focusing on the so-called P1 band (lowest-energy electronic transition) of the P3HT polaron shown on an expanded scale in Figure 1b. The spectra in both panels are normalized to the height of the absorption maximum near 0.4 eV, and further experimental details can be found in the Supporting Information.

The red curves in Figure 1 show the results when pure DCM is used as a dopant processing solvent. As is well known, doping P3HT this way leads to a reduced intensity of the neutral P3HT exciton absorption near 2.3 eV (black curve) as electrons are removed from the polymer valence band. Doping also leads to the appearance of a new band with two sharp vibronic features near 1.5 eV, which are representative of the F₄TCNQ anion produced by ICT, along with the so-called P2 absorption band of the oxidized polymer that appears in the same energetic location. Finally, doping and ICT lead to a new absorption with peaks at 0.16 and ~0.4 eV, corresponding to the infrared active vibrations (IRAV) band and the P1 band of the hole (or polaron) on the polymer, respectively. The relative intensities of the P2/F₄TCNQ⁻ peak, the P1 band, and the remaining neutral P3HT absorption are all comparable in magnitude. In a previous work, we found that, with sequential doping, there is a maximal amount of F₄TCNQ that can be intercalated into a pre-existing polymer film, no matter how high the doping solution concentration. The spectral signature for reaching this "saturation doping" is seen when the P1, P2/ F₄TCNQ⁻, and neutral P3HT bands are all comparable in absorbance, as is the case for these samples.³³

With the exception of the film doped using pure CF, the other colored curves in Figure 1 show that using blends of DCM and CF to dope the P3HT film with F₄TCNQ leads to the generally observed ICT doping behavior. However, for the solvent blend composed of 80% CF and 20% DCM (blue curves), there is a noticeable increase in absorption near 0.7, 2.0, and 3.3 eV, which further increase when casting F₄TCNQ from pure CF (purple curves). The three new features all match well with what has been observed previously for CTC formation by Jacobs et al. for this system when hot solution mixtures of P3HT and F₄TCNQ and hot substrates and pipette tips were used to create doped films.²⁶ These workers were able to isolate a structurally novel polymorph associated with these electronic features,²⁶ which we show below is also present in our films doped sequentially from CF. Thus, Figure

1 shows that changing the solvent blend used for doping allows for control over the relative amount of CTC formation.

The results in Figure 1 can further be compared to work from Thomas et al., who showed that F₄TCNQ doping can produce CTC states in a polythiophene derivative whose conjugated backbone is identical to that of P3HT, but with branched ethyl-hexyl side chains.²⁷ The bulkier side chains prevent F₄TCNQ molecules from residing in their typically preferred location in the lamellar regions of the P3HT crystallites, leading to an absorption spectrum that resembles that seen with hot solvent casting by Jacobs et al.²⁶ and that of the purple curves in Figure 1. Thus, the UV-Vis-NIR spectrum in Figure 1a strongly suggests that the elevated solubilizing power of CF has a similar effect to hightemperature-prolonged solvation of both species, allowing them to assemble into a polymorph with π -stacked charge transfer interactions that are separate from the typical ICT geometries seen for doped conjugated polymers. In addition, the relative intensity of the CTC absorption features to the P1 polaron peak seen for the pure CF processing condition further indicates that a substantial fraction of the F₄TCNQ molecules in the film are no longer undergoing ICT and are instead doping via CTC formation. It is tempting to attempt to use the measured spectra to quantitatively extract information about the overall doping level and/or the ratio of ICT to CTC carriers for each set of processing conditions. However, because these films are doped via sequential deposition, we do not quantitatively know the overall doping level. We have established previously 17 that there is overlapping peak intensity of the F₄TCNQ anion with other absorbing species, and unfortunately, we do not know the cross section for any of the absorbing species in doped P3HT films. This makes it problematic to use absorption spectroscopy directly to quantify the relative amounts of the different doped species. Despite this, we will show in Section 3.2, below, that we can obtain good estimates of carrier concentrations from spectroscopy via a more indirect method.

Figure 1b also shows that increasing CF content produces a monotonic redshift of the main P1 absorbance peak near 0.4 eV that is concomitant with an increase in the relative intensity of the IRAV modes located near 0.16 eV, as highlighted by the black arrows. These two spectral features are hallmarks of greater polaron delocalization and increased carrier mobility. 21,42,43 We believe that this results from a solvent annealing effect. CF (b.p. = 61.2 °C) has a higher boiling point than DCM (b.p. = 39.6 °C), and the extra drying time and increased P3HT solubility during spin coating likely give P3HT crystallites more time to order, as we will demonstrate using GIWAXS data in Section 3.3 below. It is also possible that the more soluble disordered polymer regions, corresponding to more blue-shifted P1 absorption, are the most likely to be dissolved away upon exposure to CF. Together, this means that increasing CF content when depositing F₄TCNQ both increases the formation of CTCs but also makes those remaining carriers produced via ICT even more mobile.

3.2. Quantifying CTC Formation Using the F_4TCNQ C $\equiv N$ IR Stretching Modes. Two features make the F_4TCNQ C $\equiv N$ vibrational modes particularly well suited for studying CTC formation: (1) the fact that the frequency of C $\equiv N$ stretches are known to be highly sensitive to the local coulombic environment ^{44,45} and (2) the fact that the C $\equiv N$ stretch frequencies occur near 2200 cm $^{-1}$, which places them in an IR spectral window that is largely absent of other

vibrational modes. Although neutral F_4TCNQ has a vibration that weakly absorbs near 2227 cm⁻¹, the fully anionic species produced by ICT undergoes a mode softening, bringing the vibrational frequency down to ~2190 cm⁻¹, as shown in Figure 2a. Because the energy of the C \equiv N stretching mode is highly dependent on the charge state of the dopant molecule, FTIR is better suited than UV–Vis–NIR for quantifying the abundance of partial charge transfer states since the F_4TCNQ stretching vibrational energy associated with CTCs appears at intermediate stretching frequencies just above 2200 cm⁻¹. 26,28,29 For the case when pure CF is used as the casting solvent, the purple curve in Figure 2a shows a well-defined peak at 2201 cm⁻¹, clearly revealing the presence of a large fraction of CTC states for this dopant casting condition.

Consistent with the electronic indications of CTC formation from the UV–Vis–NIR in Figure 1, Figure 2a shows that, as the fraction of CF is increased in the dopant casting solvent blend, the fraction of CTC states in the doped films also increases. Surprisingly, however, even when using pure DCM as the dopant casting solvent, the presence of the CTC peak near 2201 cm⁻¹ never disappears. The ratio of CTC to ICT states, taken from the integrated peak areas in the IR spectrum and plotted as the blue curve in Figure 2b, reaches 0.04, but never zero. This suggests that, for sequential solution doping, there is always a small population of CTC states formed alongside the more predominant ICT phase when doping P3HT with F4TCNQ.

It is worth pointing out that the corresponding electronic transitions for the small fraction of CTC states produced at low CF fractions are not readily identifiable in the corresponding UV–Vis–NIR spectra. This is due to the already crowded nature of the electronic spectrum, the small population of CTCs generated for these doping conditions, and the fact that the CTC electronic absorption features likely have lower cross sections than the corresponding ICT features. However, using the integrated area peak fits from the FTIR spectra, we find that the CTC content can be controllably varied in these doped films by a factor of just over 10 as the fraction of CF in the dopant casting solvent is tuned from zero to 100%.

To better understand how the presence of CTCs affects the electronic properties of F_4TCNQ -doped P3HT films, we also probed the in-plane conductivity of the various doped P3HT films. Figure 2b (red squares) shows the electrical conductivity of the films as a function of CF composition in the doping solvent blend. A monotonic decrease in electrical conductivity is observed, going from 5.6 ± 0.3 S cm⁻¹ when using pure DCM, down to 2.3 ± 0.3 S cm⁻¹ when using pure CF as the casting solvent, a $\sim 60\%$ reduction in electrical conductivity.

It is well known that the electrical conductivity is given by, $\sigma = pe\mu$, where μ is the free carrier mobility, p is the free carrier density, and e is the fundamental charge. Recently, we performed an analysis based on AC Hall effect measurements to show that, for P3HT, the energetic location of the P1 polaron band is strongly correlated with the free charge carrier mobility. Thus, we can use this correlation, along with the measured electrical conductivity and P1 peak position, to estimate the free carrier density and mobility in our doped P3HT films as a function of CF fraction in the solvent used to infiltrate the F₄TCNQ dopant. The precise way we accomplish this is described in both ref 24 and the Supporting Information, and the results are shown in Figure 2c.

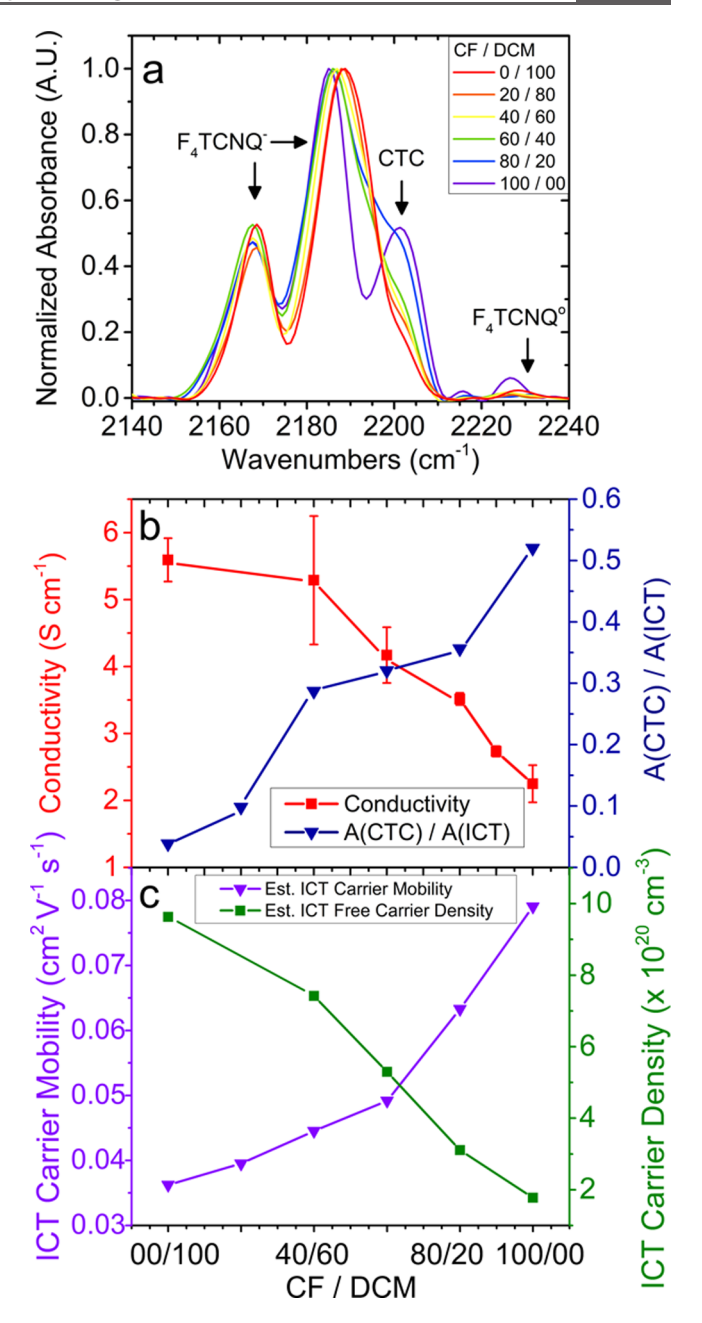


Figure 2. (a) Infrared absorbance of the C≡N stretching modes of F₄TCNQ-doped P3HT films as the dopant is introduced sequentially from solvent blends containing various CF/DCM ratios. The CTC peak at 2201 cm⁻¹ shows a monotonic increase in relative amplitude as the fraction of CF is increased for the doping solvent. (b) Electrical conductivity (red squares) plotted against the fraction of CF in the doping solvent blend. A monotonic decrease in conductivity is observed as an increasing proportion of CF is used in the doping solvent despite the fact that the carriers produced by ICT are becoming more mobile. The ratio of the integrated infrared peak area for the CTC peak at 2201 cm⁻¹ to that of the integrated peak area of the central ICT infrared band located near 2185 cm⁻¹ (blue triangles), both taken from the data in panel (a). (c) Estimated ICT carrier mobility (purple triangles), calculated as described in the Supporting Information and ref 24 using the energy of the P1 polaron band peak absorbance. The estimated ICT carrier density (green squares) was calculated from the estimated mobility and the experimentally measured electrical conductivity. Clearly, the presence of CTC states is strongly anticorrelated with the doped film ICT carrier density.

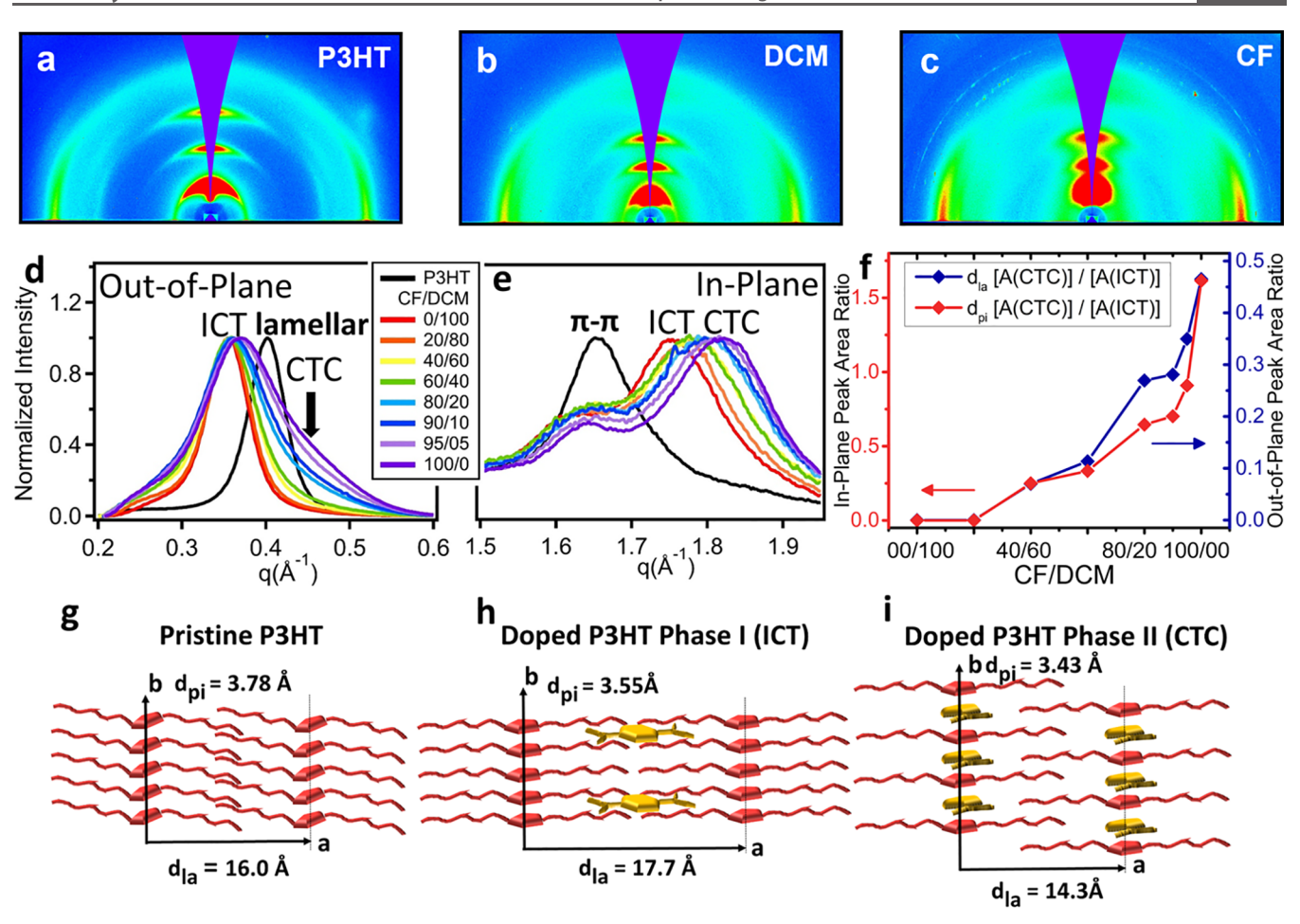


Figure 3. 2D GIWAXS diffractograms for films of (a) pristine P3HT, (b) P3HT sequentially doped with F_4 TCNQ from 100% DCM, and (c) doped from 100% CF. The polymer chains in all samples maintain their edge-on orientation, but the peak positions, widths, and texture all change with doping and with the particular doping solvent composition. (d) Normalized out-of-plane and (e) in-plane integrations of thickness-normalized 2D GIWAXS diffractograms of P3HT sequentially doped with F_4 TCNQ from blend solvents with different ratios of CF and DCM. The in-plane scattering from the π-stacking region in panel (e) shows a continuous shift to higher q and a broadening of the peak width as the CF fraction is increased. The out-of-plane scattering in the lamellar region in panel (d) shows that, with increasing CF ratio, a new peak appears at higher q. (f) Integrated GIWAXS peak area ratios for the CTC (phase II) relative to the ICT (phase I) structures, for both the out-of-plane lamellar (blue points) and in-plane π-stacking (red points) peaks. The structural trends match with what we deduced from the infrared C \equiv N stretch vibrations in Figure 2b. (g) Cartoon of the pristine P3HT crystal structure showing that the b direction is not precisely parallel to the π -stacking direction. (h) Cartoon of the ICT (phase I polymorph) structure of doped P3HT, showing how F_4 TCNQ resides in the lamellar region of the crystallites and rearranges the unit cell, resulting in a decreased π distance ($d_{\rm pi}$) and increased lamellar distance ($d_{\rm la}$). (i) Cartoon of the CTC (phase II polymorph) structure of P3HT doped with F_4 TCNQ. Because the incorporation kinetics are changed when CF is used as the dopant solvent, F_4 TCNQ is capable of π -stacking with the P3HT backbone, forming an interdigitated lamellar structure with decreased lamellar and tighter π -stacking distances.

The purple triangles in Figure 2c show that, as the fraction of CF in the dopant solution is increased, the estimated free carrier mobility actually increases from 0.036 cm 2 V $^{-1}$ s $^{-1}$ for pure DCM up to 0.8 cm 2 V $^{-1}$ s $^{-1}$ when using pure CF. These values are well within the range of Hall mobilities that have been measured previously for similarly doped P3HT films. 21,23,24 Given that the electrical conductivity decreases with increasing CF fraction, the increase in free carrier mobility reflects a strong decrease, over 80%, in the density of free carriers produced by ICT, shown as green squares/right axis in Figure 2c. We note that we spent a great deal of time attempting to quantify the CTC carrier concentration in these films from absorption, but this is challenging to do accurately because we do not know the cross sections of either the vibrational or electronic transitions of either the F₄TCNQ anion or the CTCs. However, if we assume a similar total dopant loading density across this series of doped P3HT

samples, then the drop in free carrier concentration suggests a CTC dopant concentration of roughly $8\times 10^{20}~\text{cm}^{-3}$. Thus, free carriers created by ICT become more mobile with the use of CF as a doping solvent, but the overall electrical conductivity still drops due to the fact that free carriers produced by integer charge transfer are lost via conversion into CTCs.

Overall, IR spectroscopy and electrical conductivity show that the use of solvent blends in sequential doping affords a high degree of control over the relative population of CTCs compared to ICTs. Simply changing the amount of CF in the solvent used to infiltrate F₄TCNQ into a P3HT film is enough to control the amount of CTCs present, allowing us to study their electronic, vibrational, and structural properties. The fact that we cannot entirely eliminate CTC formation, however, even using pure DCM as the dopant casting solvent, means

that there is still significant room to improve the electrical properties of doped conjugated polymer films.

3.3. The Structure of P3HT:F₄TCNQ CTCs via Grazing-Incidence Wide-Angle X-ray Scattering. To understand the local structures of the crystalline ICT and CTC states, we used 2D GIWAXS to probe films sequentially doped from different composition CF/DCM solvent blends. P3HT is well known to lie edge-on to the substrate, with its side chains oriented normal to the substrate and its π - π stacking oriented in the plane of the film (Figure 3a). Pristine P3HT has a monoclinic crystal structure where the angle of π - π stacking is tilted with respect to the unit cell b axis (Figure 3g). 46

Upon doping P3HT with F_4TCNQ , Figure 3b shows that the overall edge-on orientation is preserved, while Figure 3d (red curve labeled ICT) shows that the lamellar scattering peak shifts to a lower q. The red curve in Figure 3e shows that the $\pi-\pi$ stacking peak splits into two, with one peak remaining near the original location and a new peak appearing at a higher q. $^{7,21-24,35}$ All of these shifts result from a rearrangement of the P3HT crystal structure upon doping, caused by the incorporation of F_4TCNQ into the side-chain regions of the P3HT crystallites. The added F_4TCNQ volume causes a reduction in the tilting of the $\pi-\pi$ stacking direction with respect to the b axis and thus a reduction in the π spacing, as shown in Figure 3h. 22

The fact that the dopants prefer to reside in the polymer lamellae (even for dopants that are physically larger than the lamellar spacing) 23,24 is important for helping to physically separate polarons from their counterions following ICT. This is because the low dielectric constant of organic semiconductors does a poor job of screening the interaction between the charge carriers on the polymer backbone and the dopant counteranion. When the dopant counterion in a crystallite is located among the polymer side chains, it is physically as far from the holes on the polymer backbone as possible, allowing the holes to move more freely. Despite the preference for dopants to occupy the lamellae and thus be physically separated from the polaron, it has been estimated that only 5 to 10% of holes generated by doping P3HT with $\rm F_4TCNQ$ become free charge carriers. $\rm ^{14,24}$

In contrast to the ubiquitous formation of ICT states when paired with semiconducting polymers, F_4TCNQ usually shows fractional charge transfer when combined with small organic donor molecules, forming CTCs as mentioned earlier. The donor molecules, forming cTCs as mentioned earlier. The donor charge transfer, the degree of charge transfer can vary from 0 to 1^{13} Similarly, both experimental and theoretical work show that conjugated oligomers also have a tendency to π -stack with F_4TCNQ , which means that oligomers show a very different structural behavior when compared to their polymeric counterparts composed of the same monomer.

This leads us again to the question of why CTCs form readily in charge-transfer salts, but much less so in doped conjugated polymers. As discussed above, increasing the polymer solubility by casting at high temperatures or forcing dopants out of the lamellae with branched side chains can facilitate CTC formation. Moreover, Neelamraju et al. found that CTC formation can be the preferred doping mechanism in regiorandom P3HT, which is a highly amorphous material compared to the regioregular P3HT material studied in this work.

The spectroscopic characterization presented above shows evidence for the co-existence of ICT and CTC states in P3HT

films sequentially doped with F_4TCNQ using CF/DCM solvent blends. Here, we draw similar conclusions based on structural evidence derived from GIWAXS. We find that changes in the diffraction patterns emerge as the CF ratio of the doping solvent increases, as seen in Figure 3a–c (intermediate CF/DCM ratios are shown in Figure S6 in the Supporting Information). As the fraction of CF in the doping solvent is increased, both the peak positions and widths evolve. In particular, when P3HT is doped using CF (Figure 3c), the scattering shows unusual broadening of both the lamellar and π -stacking peaks. In addition, thickness-normalized data in Figure S8 shows that the P3HT crystallite orientation becomes less edge-on with higher CF ratios in the doping solvent.

To better display the structural changes that take place upon doping, Figure 3d,e shows radially integrated 1D curves from the corresponding 2D scattering patterns. Panel (d) shows normalized out-of-plane integrations for the lamellar peak for different doping solvent blends. When P3HT is doped with F4TCNQ using DCM as the casting solvent (red curve), the peak from the pristine material (black curve) shifts to a lower q (higher d spacing), as expected for intercalation of F4TCNQ into the crystalline lamellae. ^{21,22} As the fraction of CF in the doping solvent increases, the ICT lamellar peak remains in the same shifted position, but a shoulder grows in at a higher q, which fits best to a single new peak appearing around 0.44 Å⁻¹ (see Figure S7a in the Supporting Information for more details on fitting). This new peak can be assigned to the fundamental lamellar spacing of the CTC phase. ²⁶

Figure 3e shows the normalized in-plane integration in the π -stacking region for the same series of doped P3HT films. Here, we see that when pure DCM is used as the doping solvent (red curve), the original undoped π peak (black curve) decreases in intensity while a new π peak appears at 1.66 Å⁻¹, as expected when F₄TCNQ occupies the lamellar region of the crystallites. As the fraction of CF in the doping solvent increases, the doped-phase π -stacking peak appears to shift to a higher q and slightly broadens. A detailed analysis shows that this results from changes in intensity of two underlying peaks: the original doped lower q peak at 1.66 Å⁻¹ (ICT peak) decreases in intensity, while a second peak from the CTC phase appears at 1.84 Å⁻¹ when high fractions of CF are used (see Figure S7b for fits).

Both the out-of-plane lamellar peak at 0.44 Å⁻¹ and the inplane π -stacking peak at 1.84 Å⁻¹ closely resemble those of the CTC polymorph described by Jacobs et al.²⁶ This provides structural confirmation that tuning the fraction of CF in the doping solvent controllably introduces a second polymorph of doped P3HT (labeled phase II in Figure 3i), which co-exists with the more familiar ICT phase I structure (Figure 3h). Since the new phase II shows a decrease in lamellar packing distance as well as a further decrease in π - π distance, we assign it to a CTC structure where F₄TCNQ π -stacks with thiophene rings on the P3HT backbone and the side chains become further interlocked.²⁶

We note that, in previous works, ICT was incorrectly postulated to take place via a π -stacking arrangement. This makes the structural data presented here and in ref 26 interesting in that we can definitively correlate P3HT polymorphs with the F₄TCNQ dopant occupying either the lamellar or the π -stacks to two unique charge transfer interactions with distinct spectroscopic and electronic properties.

With the caveat that GIWAXS only reports on the crystalline regions of a sample (and we know there can be significant amounts of F_4TCNQ in the amorphous regions at high doping concentrations 23,53), we can use the ratio of the integrated peak areas for each of the two phases to estimate their relative abundance. Figure 3f shows the ratio of the CTC and corresponding ICT peaks for both the lamellar (blue data points) and π -stacking (red data points) regions. The ratios of the two different peaks change in a similar fashion with increasing CF fraction, verifying that they are indeed reporting on the same new phase.

We believe that this results from the fact that CF's high dissolving power is capable of swelling and disrupting the P3HT crystallite structure to a much greater extent than DCM during the sequential doping process. This disruption allows F_4TCNQ to intercalate between the P3HT π -stacks, producing the phase II polymorph associated with CTC doping. The appearance of the new phase monitored by GIWAXS also closely matches that monitored by the infrared absorbance of the C \equiv N stretch of the F_4TCNQ , as shown in Figure 2b. Interestingly, the diffraction peak area ratio in Figure 3f increases somewhat more gradually than the IR peak area ratio, suggesting that CTC states formed at lower CF fractions occur with higher probability in disordered regions of the polymer, and thus affect the GIWAXS data less strongly than the IR absorption.

One additional question is whether the redshift in the P1 band observed in Figure 1b can be correlated with structural changes observed in GIWAXS. Figures S6 and S7 in the Supporting Information show a systematic decrease in ICT scattering intensity with increasing CF fraction at all compositions below 100% CF. This decrease is likely due to the conversion of ICT states to CTC states. At 100% CF, the intensity jumps up, indicating that, despite significant CTC formation, the total crystallinity is also increasing. The fact that high CF fractions can dramatically crystallize formerly amorphous regions of the polymer is compatible with the idea that smaller amounts of CF can more subtly increase order in the already crystalline regions, helping to explain the redshift of the P1 peak observed in Figure 1b.

3.4. Dopant Infiltration Method and CTC Formation. Now that we have established that CF content can be used to tune the relative amounts of ICT and CTC formation in F_4TCNQ -doped P3HT films, we next explore the effects of different dopant infiltration methods. In a previous work, our group performed a head-to-head comparison of sequential doping using solution vs evaporation deposition.³³ Evaporation, or vapor doping, involves exposing a pre-cast polymer film to a flux of dopant vapor created by sublimation. We found that vapor doping is every bit as effective as solution doping, even for very thick polymer films, and that vapor doping does a slightly better job of preserving the underlying crystallinity of the polymer film than solution doping.³³

Figure 4 shows the IR absorption of two sets of sequentially doped P3HT films; one set based on underlying films of 110 nm thickness (red curves) and a second set based on underlying films of 400 nm thickness (blue curves). We have shown previously that, due to the spin-coating conditions for the pure material, the 400 nm-thick films have a higher total crystallinity compared to the 110 nm-thick films.³³ We then doped each set of films with F₄TCNQ both by solution processing (solid curves), using 100% DCM as a casting solvent (1 mg mL⁻¹) as well as by vapor deposition (dashed

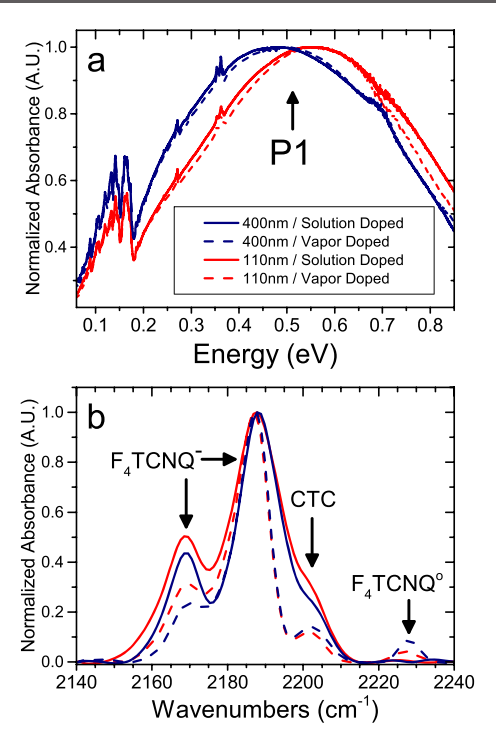


Figure 4. (a) FTIR absorption spectra normalized against max P1 intensity for a set of 400 nm-thick (blue curves) and 110 nm-thick (red curves) doped P3HT samples. Solid curves designate films treated by sequential solution doping with F_4TCNQ at 1 mg/mL from DCM. Dashed curves designate films doped with F_4TCNQ by vapor transport. (b) Inset view of the same set of spectra shown in (a) replotted in the wavenumber range for the $C \equiv N$ stretching modes. In panel (a), the small set of peaks centered near ~ 0.27 eV on the P1 spectrum correspond to absorption of the F_4TCNQ vibrational modes.

curves) in an evaporator equipped with a QCM thickness monitor to achieve comparable doping levels. The increased IRAV absorption and redshift of the P1 band of the 400 nm-thick films seen in Figure 4a make it clear that the thicker films have a greater degree of polaron delocalization and thus increased degree of order. Figure 4a also shows that choice of sequential doping method has almost no effect on the degree of delocalization.

Figure 4b shows the FTIR spectra of these same films in the F₄TCNQ C≡N stretching region. Unlike the electronic absorption, the FTIR data shows pronounced differences depending on the sequential processing method employed. The biggest difference is in the relative amplitude of the CTC band at 2201 cm⁻¹, which is significantly higher for solution doping with DCM compared to evaporation doping. This suggests that evaporation doping goes further toward eliminating undesirable CTC formation than solution doping, independent of the initial degree of film crystallinity. From the perspective of kinetics, solution doping is much more effective at disrupting the existing P3HT π -stacks and thus at facilitating insertion of dopants in π -stacks and CTC formation. On the other hand, vapor transport is a minimally invasive processing technique during which P3HT π -stacks are less likely to be disrupted, causing CTC doping to be largely relegated to the amorphous polymer regions. In addition, the vapor-doped films show remarkably narrow ICT C≡N stretching modes, suggesting a more homogeneous population of ICT states. Overall, the data show that the choice of doping method can

also control the extent of CTC formation, which may be important for many applications.

3.5. The Role of P3HT Crystallinity in CTC Formation.

One of the strongest advantages of sequential doping is that it allows for a degree of control over the total crystallinity of a doped polymer film. Since the polymer layer is deposited first in sequential doping, the processing conditions (choice of solvent, spin speed, thermal annealing, etc.) can be chosen to enhance or reduce crystallinity as desired. In a previous work, we examined how controlling the crystallinity of pre-cast P3HT films affected the electrical and optical properties after sequentially doping with F₄TCNQ.

Here, we follow those same methods to prepare P3HT films of identical thickness with three different degrees of crystallinity, whose (undoped) UV-Visible absorption spectra are shown in Figure 5a. First, we cast the initial P3HT film from CF (prior to doping), which is a rapidly evaporating solvent that produces substantially more disordered, lower crystallinity films than traditional aromatic solvents used for polymer deposition (teal curve). The relatively low crystallinity is easily verified by the lack of vibronic structure in the UV-Vis^{54,55} as well as by GIWAXS.²¹ Second, we cast the P3HT films using our standard high boiling point solvent odichlorobenzene (ODCB) (orange curve), producing highercrystallinity films, as evident by both GIWAXS²¹ and by the presence of vibronic structure in the UV-Visible absorption spectrum. Finally, very high crystallinity films were obtained using a specially synthesized batch of P3HT with nearly 100% regioregularity, ⁵⁶ also cast from ODCB (blue curve).

Figure Sb shows the UV–Vis–NIR absorption spectra of the same three films as panel (a) after solution sequential doping with F₄TCNQ using pure DCM (1 mg mL⁻¹) as a casting solvent. As expected, the films with higher crystallinity show a red-shifted main P1 band near 0.4 eV and an increased relative IRAV band intensity near 0.16 eV.^{21,23,24,42,43} The electrical conductivity, carrier mobility, free carrier concentration, and GIWAXS of films produced this way all have been discussed in our previous work; the electrical conductivity of the most crystalline film conditions is roughly seven times higher than that of the least crystalline, as a direct result of improved carrier mobility with increased crystallinity.²¹

Figure 5c shows the corresponding FTIR absorption spectrum of the F₄TCNQ C≡N stretching modes in these same three doped P3HT films. Interestingly, the main (ICT) anion absorption band shifts position from 2191 cm $^{-1}$ in the least crystalline film (P3HT cast from CF) to 2185 cm $^{-1}$ in the most crystalline film (100% RR P3HT). This suggests that the position of the ICT vibronic absorption band depends directly on the degree of overall crystallinity, with the more ordered environments producing a red-shifted vibronic band; we will explore this observation in more detail in future work.

In addition to the shift of the anion absorption associated with ICT, the data in Figure 5c show the distinct presence of the CTC peak in all three films, as evidenced by its vibronic absorption near 2201 cm⁻¹. The correlation is clear: the film with the lowest overall crystallinity has the largest fraction of CTCs, and vice versa for the most crystalline film. Given that the CTC requires π -stacking of the dopant and polymer, which is kinetically difficult to achieve in crystallites, it makes sense that CTC formation is favored in more disordered, amorphous films, where the requisite π -stacking geometry is easier to achieve.

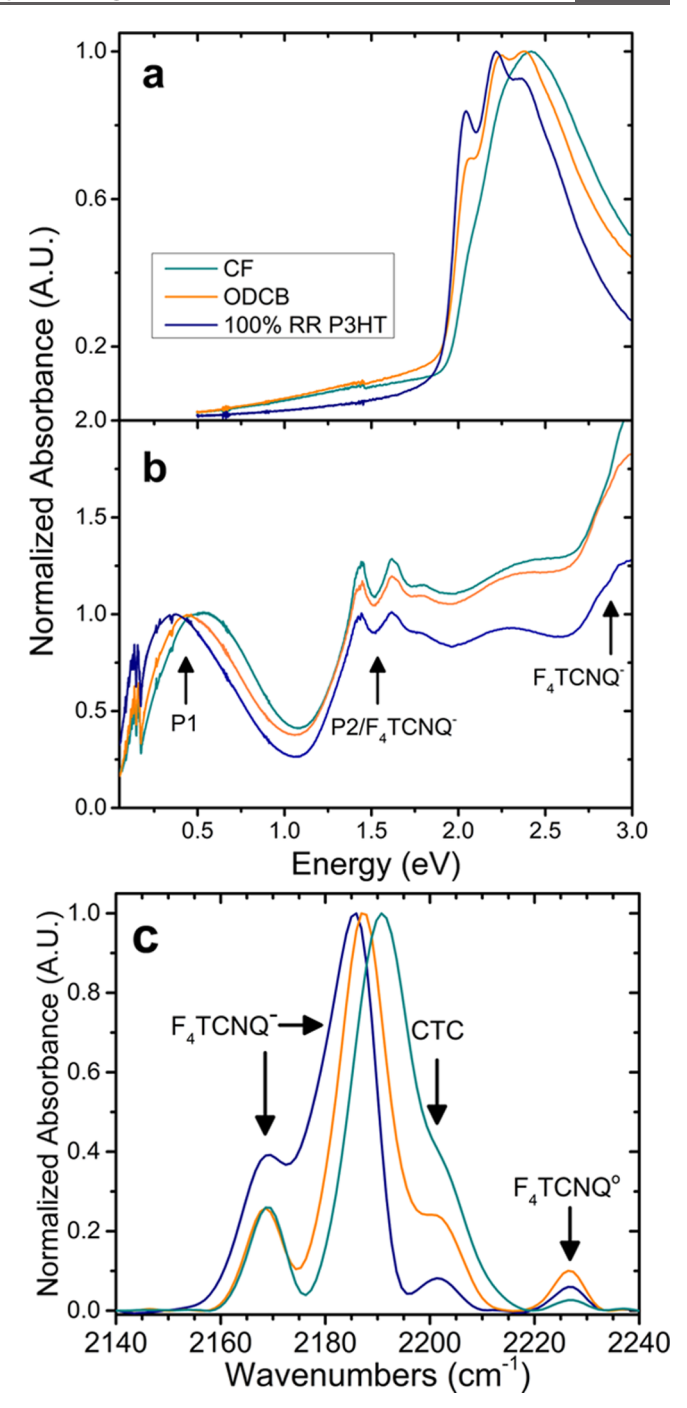


Figure 5. (a) UV—vis absorption spectrum of three different P3HT films with increasing crystallinity controlled by the evaporation kinetics of the solvent used to cast the film or the degree of polymer regioregularity. (b) UV—vis—NIR/FTIR combined spectrum for the same set of films after sequential solution doping with F_4TCNQ from DCM (1 mg mL⁻¹), normalized at the P1 band. (c) Vibrational spectra for the F_4TCNQ C \equiv N stretching mode for the same three films. The CTC peak near 2201 cm⁻¹ clearly shows that lower polymer crystallinity is associated with forming more CTC states.

3.6. Thermal Annealing and the Stability of CTC States. The question of the relative thermodynamic stability of CTC and ICT phases in doped conjugated polymer films has also been a topic of considerable interest. Watts et al. recently argued that CTC states in P3HT films are thermodynamically preferred, ²⁹ while Jacobs et al. showed

that the CTC polymorph in their samples rapidly degraded when exposed to light or air, suggesting that the CTC states are kinetically unstable. More recently, Zapata-Arteaga et al. investigated CTC formation following extended thermal annealing of vapor-doped conjugated polymer films and ultimately concluded that samples rich in the CTC phase are more thermally stable. 30

Because of the control over CTC production afforded by our solvent blend method, we have also addressed this question here by exploring the effects of thermal annealing. Our goal is to understand if the CTC phase, once formed, is only kinetically stable or is in fact the thermodynamically preferred phase. It is known that F₄TCNQ can thermally desorb from doped P3HT films upon exposure to higher temperatures, leading to chemical dedoping of these films. Thus, to test the stability of the CTC phase, we employed only modest heating for a short duration. Utilizing the full span of CF/DCM solvent blend ratios, doped P3HT films were placed on a hot plate at 80 °C for 1 to 5 min in a nitrogen atmosphere. The samples were removed promptly after the indicated time and allowed to cool to room temperature prior to analysis.

Figure 6 shows the results of thermally annealing our pure CF-doped films, which contain the highest fraction of CTC states, for different durations of time.

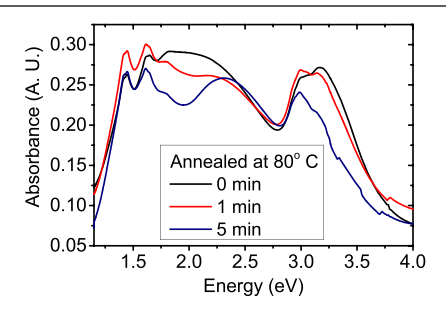


Figure 6. UV–Visible absorption spectra of P3HT films sequentially solution doped with F_4TCNQ (1 mg mL $^{-1}$) using 100% CF as the dopant casting solvent. The red curve represents a short annealing time of 1 min, while the blue curve represents annealing for 5 min. Thermal annealing at 80 °C was carried out in a nitrogen glovebox. Brief annealing for 1 min shows increased absorbance of the F_4TCNQ anion peaks near 1.5 and 3.0 eV and decreased CTC absorption near 2.0 eV, indicating a conversion of the CTC phase to the ICT phase without a significant loss of total doping. More extended annealing times lead to overall dedoping as well as a complete loss of the CTC phase.

Upon heating at 80 °C for 1 min, the two vibronic absorption peaks near 1.5 eV and an additional peak near 3.0 eV all from the F₄TCNQ anion actually increase in intensity. This result is contrary to what is usually seen when annealing doped polymer films since heating typically leads to dedoping, resulting in a loss of all absorption features associated with the doped species.⁵⁷ The fact that we see increased absorption upon heating indicates that heating reverts the metastable CTC phase back to ICT. It is worth pointing out that if CTC states were simply being converted to ICT, we might expect to see isosbestic points in the spectra following different degrees of thermal annealing. However, because the thermal annealing process also causes a net dedoping of the P3HT film, the overall absorption of F4TCNQ and neutral P3HT are also changing. As such, if we continue thermal annealing at this temperature for 5 min, the resulting UV-Vis spectrum loses

overall intensity. More importantly, however, the spectrum obtained after 5 min of annealing looks quite similar to that obtained when using pure DCM as the doping solution, indicating that, at least at the level of sensitivity provided by electronic absorption, we can remove the CTC states while still leaving the majority of the ICT states intact.

Remarkably, GIWAXS patterns of the doped P3HT films (Figure 7a,b) show that the new CTC phase II polymorph reverts entirely back to the phase I P3HT ICT crystal structure upon thermal annealing. Both the lamellar peak (Figure 7a) and the π -stacking peak (Figure 7b) lose all signatures of the CTC structure. These data provide direct structural evidence that the phase II CTC polymorph is a kinetically trapped phase. Upon thermal annealing, the dopants responsible for CTC formation physically relocate in the P3HT film and revert to the more preferred integer charge transfer doping mechanism. Moreover, the thickness-normalized GIWAXS data (Figures S8c,d and S9b in the Supporting Information) show that, after low-temperature thermal annealing, both the lamellar and π -stacking peak intensities for samples doped using CF are higher than those for films processed from DCM. Even more surprising, the GIWAXS intensities for these annealed conditions are also higher than for the pristine P3HT intensity. Doped P3HT films usually show decreased lamellar peak intensities because doping usually induces some disordering. 21,23 The increased peak intensity we see after removing the CTC state (Figures 8a,b and 9a in the Supporting Information) by thermal annealing indicates that the original loss of peak intensity after doping from solvents with increasing CF fraction is due to conversion of ICT states to CTC states and not to induced disorder upon doping. Indeed, it appears that, fundamentally, CF serves as an annealing solvent during the doping process, which favorably rearranges the polymer microstructure. In the ICT state, this increased order can be observed in the P1 band (Figure 1b), and upon thermal conversion of the CTC states to ICT states, the increased order also can be clearly observed in the diffraction intensity.

Figures S8c,d in the Supporting Information also show that, after thermal annealing, the polymer crystallites in the P3HT films doped from CF become more edge-on than in unannealed films. Since the edge-on geometry is beneficial for in-plane conductivity, this could also help to explain the conductivity change after thermal annealing in Figure 7d.

The changes in structure seen by GIWAXS are directly reflected in the optical and electrical properties of the thermally annealed doped films. In the FTIR C≡N stretching region, shown in Figure 7c, the thermally annealed samples produced with DCM-rich doping solvent mixtures show little change relative to their unannealed counterparts (shown above in Figure 2a). This suggests that CTC states formed from CFpoor solvents may be isolated doping sites in amorphous regions that can more favorably form the CTC π -stacked structure. In contrast, samples fabricated with CF-rich doping solvents almost entirely lose their CTC vibrational signature at 2201 cm⁻¹ after thermal annealing. In fact, the vibrational spectra for these CF-rich, thermally annealed samples most closely resemble what was seen for our highest crystallinity predominantly ICT-doped films; in other words, annealing the samples doped from CF ultimately produces a film whose properties match the solution-doped 100% RR P3HT (Figure 5c) or the commercially available P3HT that was doped from the vapor phase (Figure 4b). The characteristic narrowing of

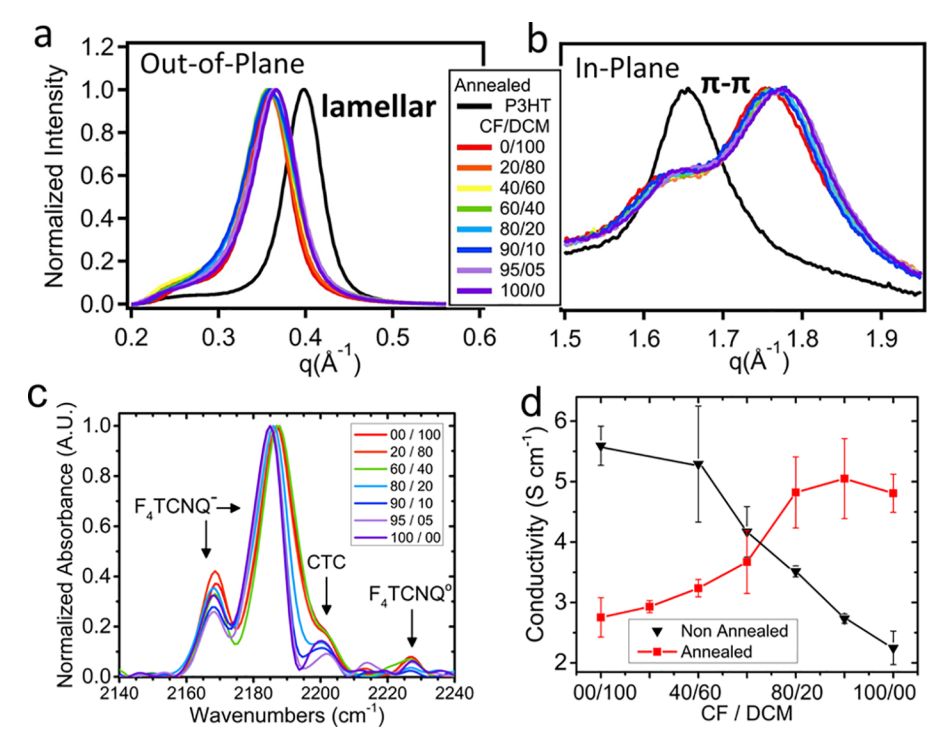


Figure 7. (a) Normalized out-of-plane and (b) in-plane integrations of thickness-normalized 2D GIWAXS diffractograms of P3HT films sequentially doped with F_4TCNQ from different ratio solvent mixtures of DCM and CF, subsequently annealed for 5 min at 80 °C. (c) Vibrational spectrum for the C \equiv N stretching mode after annealing. (d) In-plane conductivity of blend doped P3HT films prior to (black) and after annealing (red).

the principal absorption peak and relatively small intensity for the CTC peak is a common feature shared across each of these processing methods and confirms that using CF as a doping solvent actually improves the overall crystallinity for the remaining P3HT. This also provides additional evidence that ICT is thermodynamically preferred: modest heating causes a marked reduction in the CTC peak at 2201 cm⁻¹ where dopant molecules that π -stack with the P3HT backbone become free to diffuse until they can find a more stable configuration in the lamellae to undergo ICT.

Finally, Figure 7d shows the electrical conductivity of two series of identical samples doped from different solvent blends with one series subsequently being thermally annealed. As is typical for samples that use pure DCM as the doping solvent, thermal annealing decreases the electrical conductivity from 5.6 ± 0.3 to 2.8 ± 0.3 S cm⁻¹ because thermally driven desorption of the F_4TCNQ species leads to de-doping. 18,58 In contrast, for the samples sequentially doped from pure CF, annealing actually causes an increase in electrical conductivity from 2.3 \pm 0.3 to 4.8 \pm 0.3 S cm⁻¹, nearly the same value measured for unannealed DCM solvent-doped films. This behavior is also consistent with the idea that brief annealing causes F₄TCNQ molecules that were kinetically locked in the metastable CTC π -stacking phase to revert back to the ICT doping mechanism, as corroborated by the C≡N stretching spectrum and the structural changes seen with GIWAXS. The drop in conductivity from any F4TCNQ lost to desorption appears to be more than compensated for by the increased ICT carrier density and mobility due to enhanced crystallinity. Further annealing leads to additional dedoping, lowering the conductivity of all the films. An interesting crossover point exists near the 60/40 (CF/DCM) samples, which can be interpreted as a steady-state regime where the annealinginduced desorption of F_4TCNQ , the thermal conversion of CTC states into the ICT phase, and any annealing-induced changes in carrier mobility all compensate to cancel each other out.

In combination, the X-ray, FTIR, and electrical conductivity data make clear that the application of modest heating can convert the CTC phase to the more desirable ICT phase. This shows that the CTC phase is kinetically accessible only under special processing conditions but is not thermodynamically preferred, which means that the application of small amounts of heat for short treatment times may greatly improve the performance of devices based on chemically doped conjugated polymers.

4. CONCLUSIONS

Overall, our work shows that even though ICT is the preferred mechanism of charge transfer in doped conjugated polymers, fractional charge transfer, i.e., CTC formation, also plays a significant, though sometimes hidden, role. Methods like UV—Vis—NIR and X-ray diffraction are incapable of detecting the presence of CTC species when they exist in small quantities: the electronic absorption of CTCs is likely weaker than those of the ICT states, and CTCs may also be associated with primarily amorphous regions in the polymer film, making them hard to detect via X-ray diffraction. Here, we show clearly that, even in the most crystalline P3HT films, produced either using vapor doping or with 100% regioregular material, we consistently see the presence of at least some charge transfer complexes after doping with F₄TCNQ.

Why are CTCs generally harder to make and study in doped conjugated polymers than in small-molecule/oligomeric charge-transfer salts? The donor species in these charge transfer salts do not have the large aliphatic side chains needed

to confer solubility on most conjugated polymers. Thus, small molecules and oligomers tend to form co-crystals with electron acceptors that allow for the close spatial contact needed for wave function overlap and CTC formation. For conjugated polymers, there is not only much more space to place acceptors in the lamellae, but lamellar placement leads to much less disruption of the polymer crystal structure and polymer—polymer π -stacking than insertion into the π -stacks, as outlined in Figure 3g—i.

The propensity for CTCs to form in doped conjugated polymers is directly related to the degree of polymer swelling that takes place during the doping process, which in turn is linked to the fraction of amorphous regions. Indeed, we see that the relative abundance of CTCs in doped polymers increases with film swellability (and is minimized with evaporation doping), strongly suggesting that CTCs primarily reside in the disordered regions of the polymer film. This explains why CTC phases are rarely seen via GIWAXS since it is difficult to form them in large crystallites without specially controlling the processing, such as our use of CF, or via high-temperature processing as demonstrated by Jacobs et al., ²⁶ or by specifically preventing lamellar intercalation through the use of branched side chains.²⁷

The key observation in this work is that simple adjustment of the composition of the sequential processing solvent used to introduce the dopant can greatly influence the observed doping mechanism. The use of CF as a doping solvent likely redissolves the underlying polymer film and thus provides a route for the thermodynamically disfavored CTC state to form by initiating π -stacking between the dopant and the polymer in the disordered, partly dissolved state, and then preserving the kinetically trapped π -stacked structure into the solid state. This is likely the same mechanism that occurs in the hightemperature processing employed by Jacobs et al.²⁶ but should prove much easier to control for others to reproduce and further study. Moreover, we also presented a recipe-modest thermal annealing for a brief period of time—to remove CTC states and convert them to the ICT phase without significant dedoping, providing a simple way to improve the electrical performance of doped conjugated polymer films.

Moreover, our results are reassuring in that they confirm that, for conjugated polymers, doping overwhelmingly takes place by integer charge transfer. This is because, under normal sequential doping conditions, the dopants prefer the lamellae, where they remain far from the extended π -system of the polymer. Thus, the addition of side chains to conjugated polymers meant to confer favorable solubility also happens to control the preferred type of charge transfer interaction. This is consistent with conclusions we drew when exploring the doping of P3HT films with dodecaborane acceptors that are larger in size (\sim 2 nm) than the polymer lamellar spacing (\sim 1.6 nm) but still prefer to reside in the lamellar region.²⁴

Finally, when comparing dopant infiltration methods, vapor doping showed the smallest fraction of CTC states generated, independent of the degree of pre-formed polymer crystallinity. In a certain sense, vapor doping provides the absolute minimum kinetic facilitation for CTC doping, helping to explain why this method produces a notably smaller quantity of CTC states. Additionally, it seems clear that, under normal solution sequential doping conditions, the majority of CTC states are located in the amorphous polymer regions, and that the fraction of amorphous polymer will, in fact, also dictates the overall fraction of doping that takes place via the CTC

mechanism. This work suggests that, to minimize the occurrence of CTC states when sequentially doping with F_4TCNQ , one should strive for the highest crystallinity polymer possible and carry out the sequential doping process by thermal evaporation followed by brief low-temperature thermal annealing. These processing guidelines create the most conducive environment for maximizing both the equilibrium free carrier concentration as well as charge carrier mobility in these materials.

ASSOCIATED CONTENT

Supporting Information

The Supporting Information is available free of charge at https://pubs.acs.org/doi/10.1021/acs.chemmater.0c04471.

Detailed information on materials used, fabrication and doping of polymer films, optical and electrical measurements, F_4TCNQ $C \equiv N$ vibrational spectrum and peak fitting details, and GIWAXS measurements of doped polymer films (PDF)

AUTHOR INFORMATION

Corresponding Authors

Sarah H. Tolbert — Department of Chemistry and Biochemistry and Department of Materials Science and Engineering, University of California, Los Angeles, Los Angeles, California 90095-1569, United States; Occid.org/0000-0001-9969-1582; Email: tolbert@chem.ucla.edu

Benjamin J. Schwartz – Department of Chemistry and Biochemistry, University of California, Los Angeles, Los Angeles, California 90095-1569, United States; o orcid.org/ 0000-0003-3257-9152; Email: schwartz@chem.ucla.edu

Authors

Dane A. Stanfield – Department of Chemistry and Biochemistry, University of California, Los Angeles, Los Angeles, California 90095-1569, United States

Yutong Wu – Department of Chemistry and Biochemistry, University of California, Los Angeles, Los Angeles, California 90095-1569, United States

Complete contact information is available at: https://pubs.acs.org/10.1021/acs.chemmater.0c04471

Author Contributions

[¶]D.A.S. and Y.W. contributed equally to this work.

The authors declare no competing financial interest.

ACKNOWLEDGMENTS

This work was supported by the National Science Foundation under grant number CHE-2003755. Use of the Stanford Synchrotron Radiation Lightsource, SLAC National Accelerator Laboratory, is supported by the U.S. Department of Energy, Office of Science, Office of Basic Energy Sciences under Contract No. DE-AC02-76SF00515.

REFERENCES

(1) Kuik, M.; Wetzelaer, G. J. A. H.; Nicolai, H. T.; Craciun, N. I.; De Leeuw, D. M.; Blom, P. W. M. 25th anniversary article: Charge transport and recombination in polymer light-emitting diodes. *Adv. Mater.* **2014**, *26*, 512–531.

- (2) Dou, L.; You, J.; Hong, Z.; Xu, Z.; Li, G.; Street, R. A.; Yang, Y. 25th anniversary article: A decade of organic/polymeric photovoltaic research. *Adv. Mater.* **2013**, *25*, 6642–6671.
- (3) Russ, B.; Glaudell, A.; Urban, J. J.; Chabinyc, M. L.; Segalman, R. A. Organic thermoelectric materials for energy harvesting and temperature control. *Nat. Rev. Mater.* **2016**, *1*, 1–14.
- (4) Cowart, J. S., Jr.; Liman, C.; Garnica, A.; Page, Z. A.; Lim, E.; Zope, R. R.; Baruah, T.; Hawker, C. J.; Chabinyc, M. L. Donorfullerene dyads for energy cascade organic solar cells. *Inorg. Chim. Acta* 2017, 468, 192–202.
- (5) Hou, L.; Zhang, X.; Cotella, G. F.; Carnicella, G.; Herder, M.; Schmidt, B. M.; Pätzel, M.; Hecht, S.; Cacialli, F.; Samori, P. Optically switchable organic light-emitting transistors. *Nat. Nanotechnol.* **2019**, *14*, 347–353.
- (6) Liang, Z.; Zhang, Y.; Souri, M.; Luo, X.; Boehm, A. M.; Li, R.; Zhang, Y.; Wang, T.; Kim, D. Y.; Mei, J.; et al. Influence of dopant size and electron affinity on the electrical conductivity and thermoelectric properties of a series of conjugated polymers. *J. Mater. Chem. A* **2018**, *6*, 16495–16505.
- (7) Untilova, V.; Biskup, T.; Biniek, L.; Vijayakumar, V.; Brinkmann, M. Control of Chain Alignment and Crystallization Helps Enhance Charge Conductivities and Thermoelectric Power Factors in Sequentially Doped P3HT:F4TCNQ Films. *Macromolecules* **2020**, 53, 2441–2453.
- (8) Torrance, J. B.; Silverman, B. D. Charge transfer and ionic bonding in organic solids with segregated stacks. *Phys. Rev. B* **1977**, 15, 788–801.
- (9) Torrance, J. B.; Scott, B. A.; Kaufman, F. B. Optical properties of charge transfer salts of tetracyanoquinodimethane (TCNQ). *Solid State Commun.* **1993**, *88*, 971–975.
- (10) Bryan, C. D.; Cordes, A. W.; Fleming, R. M.; George, N. A.; Glarum, S. H.; Haddon, R. C.; Oakley, R. T.; Palstra, T. T. M.; Perel, A. S.; Schneemeyer, L. F.; Waszczak, J. V. Conducting charge-transfer salts based on neutral π -radicals. *Nature* **1993**, *365*, 821–823.
- (11) Ferraris, J.; Cowan, D. O.; Walatka, V.; Perlstein, J. H. Electron Transfer in a New Highly Conducting Donor-Acceptor Complex. *J. Am. Chem. Soc.* **1973**, *95*, 948–949.
- (12) Shokaryev, I.; Buurma, A. J. C.; Jurchescu, O. D.; Uijttewaal, M. A.; De Wijs, G. A.; Palstra, T. T. M.; De Groot, R. A. Electronic band structure of tetracene-TCNQ and perylene-TCNQ compounds. *J. Phys. Chem. A* **2008**, *112*, 2497–2502.
- (13) Goetz, K. P.; Vermeulen, D.; Payne, M. E.; Kloc, C.; McNeil, L. E.; Jurchescu, O. D. Charge-transfer complexes: New perspectives on an old class of compounds. *J. Mater. Chem. C* **2014**, *2*, 3065–3076.
- (14) Pingel, P.; Neher, D. Comprehensive picture of p-type doping of P3HT with the molecular acceptor F4TCNQ. *Phys. Rev. B* **2013**, 87, 115209.
- (15) Cochran, J. E.; Junk, M. J. N.; Glaudell, A. M.; Miller, P. L.; Cowart, J. S.; Toney, M. F.; Hawker, C. J.; Chmelka, B. F.; Chabinyc, M. L. Molecular Interactions and Ordering in Electrically Doped Polymers: Blends of PBTTT and F4TCNQ. *Macromolecules* **2014**, *47*, 6836–6846.
- (16) Salzmann, I.; Heimel, G. Toward a Comprehensive Understanding of Molecular Doping Organic Semiconductors (Review). *J. Electron Spectrosc. Relat. Phenom.* **2015**, 204, 208–222.
- (17) Scholes, D. T.; Hawks, S. A.; Yee, P. Y.; Wu, H.; Lindemuth, J. R.; Tolbert, S. H.; Schwartz, B. J. Overcoming Film Quality Issues for Conjugated Polymers Doped with F4TCNQ by Solution Sequential Processing: Hall Effect, Structural, and Optical Measurements. *J. Phys. Chem. Lett.* **2015**, *6*, 4786–4793.
- (18) Fuzell, J.; Jacobs, I. E.; Ackling, S.; Harrelson, T. F.; Huang, D. M.; Larsen, D.; Moulé, A. J. Optical Dedoping Mechanism for P3HT:F4TCNQ Mixtures. *J. Phys. Chem. Lett.* **2016**, *7*, 4297–4303.
- (19) Jacobs, I. E.; Aasen, E. W.; Oliveira, J. L.; Fonseca, T. N.; Roehling, J. D.; Li, J.; Zhang, G.; Augustine, M. P.; Mascal, M.; Moule, A. J. Comparison of Solution-Mixed and Sequentially Processed P3HT:F4TCNQ Films: Effect of Doping-Induced Aggregation on Film Morphology. *J. Mater. Chem. C* **2016**, 4, 3454–3466.

- (20) Kang, K.; Watanabe, S.; Broch, K.; Sepe, A.; Brown, A.; Nasrallah, I.; Nikolka, M.; Fei, Z.; Heeney, M.; Matsumoto, D.; et al. 2D Coherent Charge Transport in Highly Ordered Conducting Polymers Doped by Solid State Diffusion. *Nat. Mater.* **2016**, *15*, 896–902
- (21) Scholes, D. T.; Yee, P. Y.; Lindemuth, J. R.; Kang, H.; Onorato, J.; Ghosh, R.; Luscombe, C. K.; Spano, F. C.; Tolbert, S. H.; Schwartz, B. J. The Effects of Crystallinity on Charge Transport and the Structure of Sequentially Processed F4TCNQ-Doped Conjugated Polymer Films. *Adv. Funct. Mater.* **2017**, 27, 1702654.
- (22) Hamidi-Sakr, A.; Biniek, L.; Bantignies, J.-L.; Maurin, D.; Herrmann, L.; Leclerc, N.; Lévêque, P.; Vijayakumar, V.; Zimmermann, N.; Brinkmann, M. A Versatile Method to Fabricate Highly In-Plane Aligned Conducting Polymer Films with Anisotropic Charge Transport and Thermoelectric Properties: The Key Role of Alkyl Side Chain Layers on the Doping Mechanism. *Adv. Funct. Mater.* **2017**, 27, 1700173.
- (23) Aubry, T. J.; Axtell, J. C.; Basile, V. M.; Winchell, K. J.; Lindemuth, J. R.; Porter, T. M.; Liu, J. Y.; Alexandrova, A. N.; Kubiak, C. P.; Tolbert, S. H.; Spokoyny, A. M.; Schwartz, B. J. Dodecaborane-Based Dopants Designed to Shield Anion Electrostatics Lead to Increased Carrier Mobility in a Doped Conjugated Polymer. *Adv. Mater.* **2019**, *31*, 1805647.
- (24) Aubry, T. J.; Winchell, K. J.; Salamat, C. Z.; Basile, V. M.; Lindemuth, J. R.; Stauber, J. M.; Axtell, J. C.; Kubena, R. M.; Phan, M. D.; Bird, M. J.; et al. Tunable Dopants with Intrinsic Counterion Separation Reveal the Effects of Electron Affinity on Dopant Intercalation and Free Carrier Production in Sequentially Doped Conjugated Polymer Films. *Adv. Funct. Mater.* **2020**, *30*, 2001800.
- (25) Ghani, F.; Opitz, A.; Pingel, P.; Heimel, G.; Salzmann, I.; Frisch, J.; Neher, D.; Tsami, A.; Scherf, U.; Koch, N. Charge transfer in and conductivity of molecularly doped thiophene-based copolymers. J. Polym. Sci., Part B: Polym. Phys. 2015, 53, 58–63.
- (26) Jacobs, I. E.; Cendra, C.; Harrelson, T. F.; Bedolla Valdez, Z. I.; Faller, R.; Salleo, A.; Moulé, A. J. Polymorphism controls the degree of charge transfer in a molecularly doped semiconducting polymer. *Mater. Horiz.* **2018**, *5*, 655–660.
- (27) Thomas, E. M.; Davidson, E. C.; Katsumata, R.; Segalman, R. A.; Chabinyc, M. L. Branched Side Chains Govern Counterion Position and Doping Mechanism in Conjugated Polythiophenes. *ACS Macro Lett.* **2018**, *7*, 1492–1497.
- (28) Neelamraju, B.; Watts, K. E.; Pemberton, J. E.; Ratcliff, E. L. Correlation of Coexistent Charge Transfer States in F 4 TCNQ-Doped P3HT with Microstructure. *J. Phys. Chem. Lett.* **2018**, *9*, 6871–6877.
- (29) Watts, K. E.; Neelamraju, B.; Ratcliff, E. L.; Pemberton, J. E. Stability of Charge Transfer States in F 4 TCNQ-Doped P3HT. *Chem. Mater.* **2019**, *31*, 6986–6994.
- (30) Zapata-Arteaga, O.; Dorling, B.; Perevedentsev, A.; Martin, J.; Reparaz, J. S.; Campoy-Quiles, M. Closing the Stability-Performance Gap in Organic Thermoelectrics by Adjusting the Partial to Integer Charge Transfer Ratio. *Macromolecules* **2020**, *53*, 609–620.
- (31) Salzmann, I.; Heimel, G.; Oehzelt, M.; Winkler, S.; Koch, N. Molecular Electrical Doping of Organic Semiconductors: Fundamental Mechanisms and Emerging Dopant Design Rules. *Acc. Chem. Res.* **2016**, *49*, 370–378.
- (32) Méndez, H.; Heimel, G.; Winkler, S.; Frisch, J.; Opitz, A.; Sauer, K.; Wegner, B.; Oehzelt, M.; Röthel, C.; Duhm, S.; et al. Charge-transfer crystallites as molecular electrical dopants. *Nat. Commun.* **2015**, *6*, 8560.
- (33) Fontana, M. T.; Stanfield, D. A.; Scholes, D. T.; Winchell, K. J.; Tolbert, S. H.; Schwartz, B. J. Evaporation vs Solution Sequential Doping of Conjugated Polymers: F₄TCNQ Doping of Micrometer-Thick P3HT Films for Thermoelectrics. *J. Phys. Chem. C* **2019**, *123*, 22711–22724.
- (34) Vijayakumar, V.; Zhong, Y.; Untilova, V.; Bahri, M.; Herrmann, L.; Biniek, L.; Leclerc, N.; Brinkmann, M. Bringing Conducting Polymers to High Order: Toward Conductivities beyond 10 5 S cm 1

- and Thermoelectric Power Factors of 2 mW m 1 K 2. Adv. Energy Mater. 2019. 9. 1900266.
- (35) Patel, S. N.; Glaudell, A. M.; Peterson, K. A.; Thomas, E. M.; O'Hara, K. A.; Lim, E.; Chabinyc, M. L. Morphology Controls the Thermoelectric Power Factor of a Doped Semiconducting Polymer. *Sci. Adv.* **2017**, *3*, 24–26.
- (36) Hynynen, J.; Kiefer, D.; Yu, L.; Kroon, R.; Munir, R.; Amassian, A.; Kemerink, M.; Müller, C. Enhanced Electrical Conductivity of Molecularly p-Doped Poly(3-hexylthiophene) Through Understanding the Correlation with Solid-State Order. *Macromolecules* **2017**, *50*, 8140–8148.
- (37) Lim, E.; Peterson, K. A.; Su, G. M.; Chabinyc, M. L. Thermoelectric Properties of Poly(3-hexylthiophene) (P3HT) Doped with 2,3,5,6-Tetrafluoro-7,7,8,8- tetracyanoquinodimethane (F4TCNQ) by Vapor-Phase Infiltration. *Chem. Mater.* **2018**, 30, 998–1010.
- (38) Hynynen, J.; Kiefer, D.; Müller, C. Influence of crystallinity on the thermoelectric power factor of P3HT vapour-doped with F4TCNQ. *RSC Adv.* **2018**, *8*, 1593–1599.
- (39) Mazaheripour, A.; Thomas, E. M.; Segalman, R. A.; Chabinyc, M. L. Nonaggregating Doped Polymers Based on Poly(3,4-Propylenedioxythiophene). *Macromolecules* **2019**, *52*, 2203–2213.
- (40) Roesing, M.; Howell, J.; Boucher, D. Solubility characteristics of poly(3- hexylthiophene). J. Polym. Sci., Part B: Polym. Phys. 2017, 55, 1075–1087.
- (41) Scholes, D. T.; Yee, P. Y.; Mckeown, G. R.; Li, S.; Kang, H.; Lindemuth, J. R.; Xia, X.; King, S. C.; Seferos, D. S.; Tolbert, S. H.; Schwartz, B. J. Designing Conjugated Polymers for Molecular Doping: The Roles of Crystallinity, Swelling, and Conductivity in Sequentially-Doped Selenophene-Based Copolymers. *Chem. Mater.* **2019**, *31*, 73–82.
- (42) Ghosh, R.; Pochas, C. M.; Spano, F. C. Polaron Delocalization in Conjugated Polymer Films. *J. Phys. Chem. C* **2016**, *120*, 11394–11406.
- (43) Ghosh, R.; Chew, A. R.; Onorato, J.; Pakhnyuk, V.; Luscombe, C. K.; Salleo, A.; Spano, F. C. Spectral Signatures and Spatial Coherence of Bound and Unbound Po larons in P3HT Films: Theory Versus Experiment. *J. Phys. Chem. C* **2018**, *122*, 18048–18060.
- (44) Meneghetti, M.; Pecile, C. Charge—transfer organic crystals: Molecular vibrations and spectroscopic effects of electron—molecular vibration coupling of the strong electron acceptor TCNQF 4. *J. Chem. Phys.* **1986**, *84*, 4149–4162.
- (45) Haworth, N. L.; Lu, J.; Vo, N.; Le, T. H.; Thompson, C. D.; Bond, A. M.; Martin, L. L. Diagnosis of the Redox Levels of TCNQF 4 Compounds Using Vibrational Spectroscopy. *ChemPlusChem* **2014**, 79, 962–972.
- (46) Kayunkid, N.; Uttiya, S.; Brinkmann, M. Structural model of regioregular poly(3- hexylthiophene) obtained by electron diffraction analysis. *Macromolecules* **2010**, *43*, 4961–4967.
- (47) Sutton, A. L.; Abrahams, B. F.; D'Alessandro, D. M.; Hudson, T. A.; Robson, R.; Usov, P. M. Structural and optical investigations of charge transfer complexes involving the radical anions of TCNQ and F4TCNQ. *CrystEngComm* **2016**, *18*, 8906–8914.
- (48) Qin, Q.; Mague, J. T.; Moses, K. Z.; Carnicom, E. M.; Cava, R. J. Structure and characterization of charge transfer complexes of benzo[1,2-: B:3,4- b :5,6- b]trithiophene [C 3h-BTT]. CrystEng-Comm 2017, 19, 6355–6364.
- (49) Sato, R.; Dogishi, M.; Higashino, T.; Kadoya, T.; Kawamoto, T.; Mori, T. ChargeTransfer Complexes of Benzothienobenzothio-phene with Tetracyanoquinodimethane and the n-Channel Organic Field-Effect Transistors. *J. Phys. Chem. C* **2017**, *121*, 6561–6568.
- (50) Valencia, A. M.; Cocchi, C. Electronic and Optical Properties of OligothiopheneF4TCNQ Charge-Transfer Complexes: The Role of the Donor Conjugation Length. *J. Phys. Chem. C* **2019**, *123*, 9617–9623.
- (51) Aziz, E. F.; Vollmer, A.; Eisebitt, S.; Eberhardt, W.; Pingel, P.; Neher, D.; Koch, N. Localized Charge Transfer in a Molecularly Doped Conducting Polymer. *Adv. Mater.* **2007**, *19*, 3257–3260.

- (52) Harrelson, T. F.; Cheng, Y. Q.; Li, J.; Jacobs, I. E.; Ramirez-Cuesta, A. J.; Faller, R.; Moulé, A. J. Identifying Atomic Scale Structure in Undoped/Doped Semicrystalline P3HT Using Inelastic Neutron Scattering. *Macromolecules* **2017**, *50*, 2424–2435.
- (53) Voss, M. G.; Scholes, D. T.; Challa, J. R.; Schwartz, B. J. Ultrafast transient absorption spectroscopy of doped P3HT films: distinguishing free and trapped polarons. *Faraday Discuss.* **2019**, *216*, 339–362.
- (54) Spano, F. C. Modeling disorder in polymer aggregates: The optical spectroscopy of regioregular poly(3-hexylthiophene) thin films. *J. Chem. Phys.* **2005**, *122*, 234701–234715.
- (55) Spano, F. C.; Clark, J.; Silva, C.; Friend, R. H. Determining Exciton Coherence from the Photoluminescence Spectral Line Shape in poly(3-hexylthiophene) Thin Films. *J. Chem. Phys.* **2009**, *130*, No. 074904.
- (56) Bronstein, H. A.; Luscombe, C. K. Externally initiated regioregular P3HT with controlled molecular weight and narrow polydispersity. *J. Am. Chem. Soc.* **2009**, *131*, 12894–12895.
- (57) Jacobs, I. E.; Moulé, A. J. Controlling Molecular Doping in Organic Semiconductors. *Adv. Mater.* **2017**, *29*, 1703063.
- (58) Hase, H.; O'Neill, K.; Frisch, J.; Opitz, A.; Koch, N.; Salzmann, I. Unraveling the Microstructure of Molecularly Doped Poly(3-hexylthiophene) by Thermally Induced Dedoping. *J. Phys. Chem. C* **2018**, *122*, 25893–25899.